Bio-Medical Materials and Engineering 26 (2015) S1297–S1314
DOI 10.3233/BME-151428
IOS Press

Automatic extraction of 3D anatomical feature curves of hip bone models reconstructed from CT images

Hao Liu[a,b], Hongbo Qian[a] and Jianning Zhao[a,*]
[a]*Jinling Hospital, Department of Orthopedics, Nanjing University School of Medicine, P.R. China*
[b]*Nanjing University of Aeronautics and Astronautics, P.R. China*

Abstract. 3D anatomical feature curves (AFC) on bone models reconstructed from CT/MRI images are important in some fields, such as preoperative planning, intra-operative navigation, patient-specific prosthesis design, *etc*. Interactive extraction of feature curves on patient-specific bone models is time-consuming, has low repeatability and accuracy. This paper presents a computer graphics method to automatically extract AFC from 3D hip bone models reconstructed from CT images. A DCSS (direct curvature scale space)-based technique is firstly used to extract anatomical feature points (AFP) in every contour, using anatomical structure information as prior knowledge so that AFP are extracted and only extracted. Then, corresponding AFP are linked in different contours and AFC is generated. AFC obtained by our method were compared with those interactively extracted by three surgeons, which showed that our method is feasible (Dice coefficient: 0.94; Average symmetric surface distance: 3.97 mm). The method was also applied to identify anatomical landmarks, which showed that our method is superior to the curvature-based methods that fail to identify landmark regions or have too many redundant regions, which results in failures to subsequently label landmark regions using pre-defined spatial adjacency matrices.

Keywords: Anatomical, feature, curve, landmark, hip

1. Introduction

Anatomical landmarks are distinct places of organ/tissues [1–3]. They are usually used as position references in many applications, such as preoperative planning, virtual surgical operation, intra-operative navigation, patient-specific prosthesis design, *etc*. Automatically recognizing anatomical landmarks is an urgent task in the digital surgery field [3–11].

Most of anatomical landmarks are extremely curved regions, curves or points in geometry [1–3, 12] (see Figure 1). If some anatomical landmarks that aren't extremely curve regions exist, they can usually be localized using some extreme curvature [12]. As a matter of fact, surgeons always palpate anatomical landmarks by means of extreme curves [1, 12]. As a result, extremely curved regions are very useful means to find anatomical landmarks and are usually called anatomical feature curves (AFC). In designs, such as prosthesis design and orthopedics design, feature curves are probably more

* Address for correspondence: Jianning Zhao, Jinling Hospital, Department Orthopedics, Nanjing University School of Medicine, P.R. China. Tel.: +86 2584895781; Fax: +86 25 84895781; E-mail: zhaojianning.0207@nju.edu.cn.

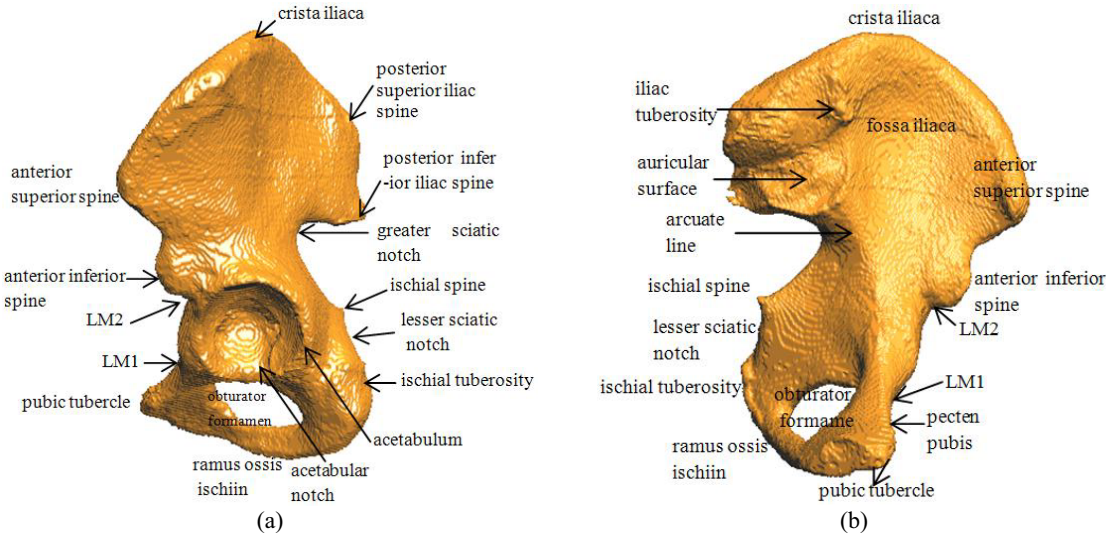

Fig. 1. Anatomical landmarks of hip bone. (a) outer side of hip bone; (b) inner side of hip bone. Where LM1 and LM2 are distinct convex/concave regions. Although they are not usually referred in anatomy, they are useful to automatically recognize anatomical landmarks in this paper.

useful than region landmarks and point landmarks because the curve net structure of a shape is an important tool for surface editing [13–15]. Furthermore, AFC of known individuals are also used to segment CT images or construct statistical models [2, 16, 17].

AFC are extremely curved regions that are also called ridge-valley lines, crest lines or feature curves in computer graphics [18–20]. Automatically or semi-automatically extracting them from discrete data, such as bone surface data reconstructed from CT images, is a challenging task, because of noises and sampling errors [18–21]. The task of the present work is to automatically extract AFC of hip bones using a computer graphics technique (DCSS—direct curvature scale space) [22, 23] and the anatomical structure of the hip bone as prior knowledge. To the best of our knowledge, there are seldom papers that incorporate shape prior information in the process of extracting feature curves.

It is kind of typical for feature extraction methods to separate extreme curvature points/curves from surfaces using classical geometrical variables, such as normal vectors, dihedral angles, curvatures, distances [18–20, 24–29], *etc*. Such methods have been used to locate anatomical landmarks such as the ones on the distal femur and on the proximal tibia [1], lumbar dimples [30], ridge-valley lines on brains [31], *etc*. Two main disadvantages of these methods are: (i) sensitivity to noise because the geometrical variables are evaluated according to the local patches of corresponding points; (ii) the extremely curved regions extracted depend on several parameter choices, for example, the curvature (or angle, distance) threshold that is necessary.

There are also methods to extract AFC using the active contour model [32]. Such methods need many given landmarks. The active contour model only links those landmarks along extreme-curvature paths. Furthermore, such methods aren't able to locate individual anatomical landmarks. The atlas method [3, 33] is also used to extract anatomical landmarks. Disadvantages of this method are: (i) the atlas has to be given beforehand; (ii) when the atlas is corrected after it is mapped to a new surface, geometrical variables of the new surface still have to be evaluated.

Compared with existing methods, the main contributions of this work are: (i) converting the problem of extracting 3D feature curves of surfaces into the problem of recognizing corners (extreme

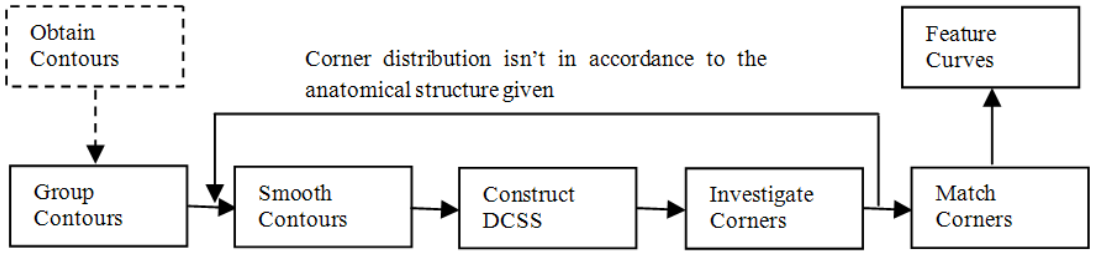

Fig. 2. Process to extract anatomical feature curves. Obtain Contours: represent 3D model as section contours; Group Contours: divide contours into several groups according to fork-like positions that can be regarded as a kind of prior knowledge; Investigate Corners: investigate whether corner distributions are in agreement to the given anatomical structure that is also prior knowledge; Track Corners: track corners in DCSS to obtain their position before contour smoothness; Match Corners: find corresponding corners between every pair of adjacent section contours. Feature Curves: Link corresponding corners to generate feature curves.

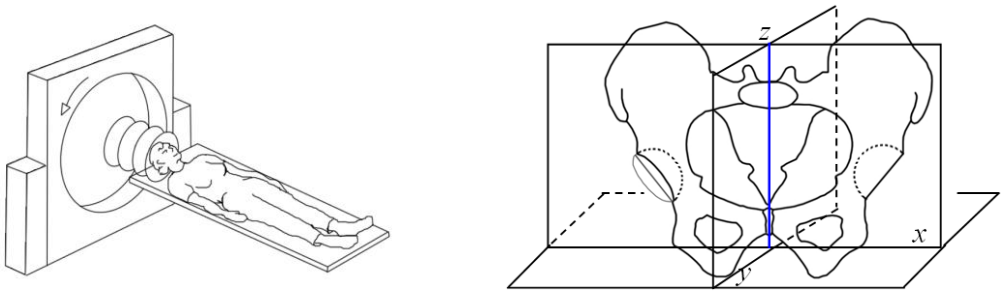

(a) (b)

Fig. 3. CT scanning coordinate system. (a) Scanning posture; (b) Coordinate axis labels.

curvature points) of planar curves, which makes the feature curve extraction process able to incorporate shape prior knowledge; (ii) there is no need for users to choose parameter values in the extraction process; (iii) our method has excellent anti-noise performance because of multi-scale smooth techniques. Note that most bone surfaces reconstructed from CT images have high noises. The feature curve extraction process in this paper is shown in Figure 2.

2. Materials and methods

2.1. Data collection

We have collected 30 hip joints in-vivo CT data of adults with normal development, 15 sets respectively for men and women. These data-sets were accumulated between 2012 and 2014 at Nanjing Jinling Hospital. The CT data-sets had been scanned by the Siemens dual-source CT machine. The number of slices of per data set ranged from 85 to 237. The resolution of every slice image was 512×512. Slice spacing ranged from 1.0~2.5 mm and pixel spacing from 0.55~0.85 mm. The scanning coordinate system was the anatomical coordinate system, as shown in Figure 3.

In order to obtain the contours of the hip bone, the valley-Bayes (V-B) detector [34] was used to segment hip bones in CT images. For cases where the femur head and the acetabulum adhere to each other and cases in which there are holes in the acetabulum surface, a special separation method [35] was applied. Figure 4 illustrates the process to obtain the contours of hip bones.

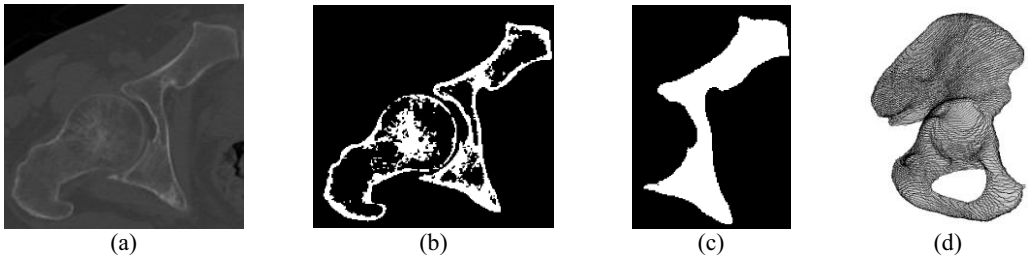

(a) (b) (c) (d)

Fig. 4. Process to obtain contours of a hip bone. (a) original CT image; (b) a black-white image obtained by the V-B detector; (c) a segmented hip from the V-B image; (d) contours of the hip bone.

2.2. Contour grouping

See Figures 1 and 4(d). Investigate the hip bone from the top to the bottom. The section contours can be divided into several groups. Contours in the same group have a similar shape and anatomical structure.

2.2.1. Outer fork-like position

In order to construct such groups, firstly the concept of the fork-like position for section contours is given. Assuming that there is a slice pair (S_{k-1}, S_k), there are respectively s contours and t contours in S_{k-1} and S_k. As far as the hip bone is concerned, $s \leq 2$ and $t \leq 2$. Without loss of generality, considering that $s=1$, $t=2$. Therefore, there are two contours $C_{k,1}$ and $C_{k,2}$ in S_k and the corresponding regions (limited by these limits) are denoted as $R_{k,1}$ and $R_{k,2}$. If $R_{k,1} \cap R_{k,2} = \Phi$, the slice pair ($S_{k-1}$, S_k) is called an outer fork-like position. There are 4 outer fork-like positions for the contours of the hip bone, as shown in Figure 5. According to these outer fork-like positions, section contours can be divided into several groups, as shown in Figures 6 and 7.

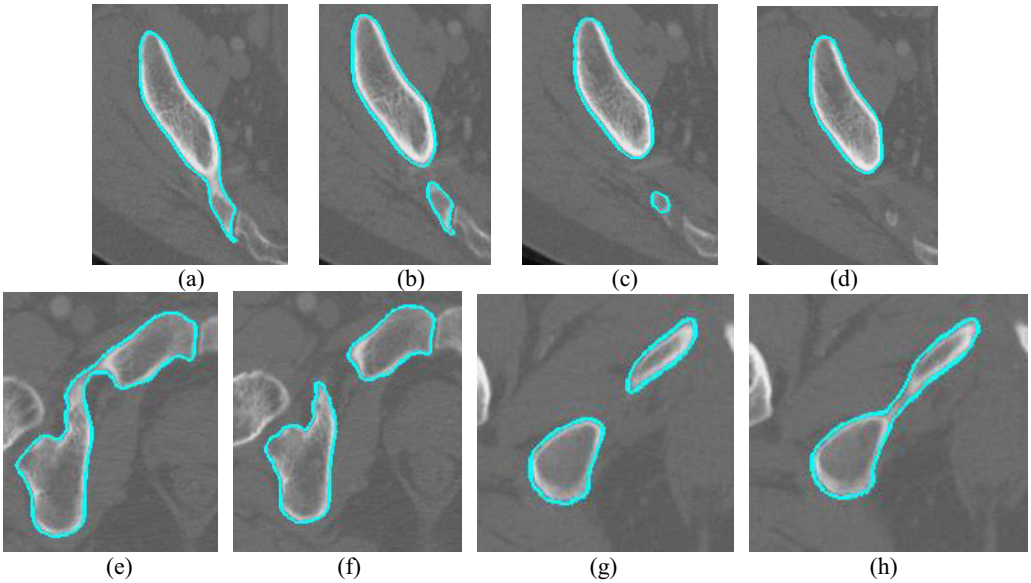

(a) (b) (c) (d)

(e) (f) (g) (h)

Fig. 5. Four outer fork-like positions of the hip bone contours. (a) and (b): greater sciatic notch; (c) posterior inferior iliac spine; (d) posterior inferior iliac spine disappears; (e) and (f): top of obturator foramen; (g) and (h): bottom of obturator foramen.

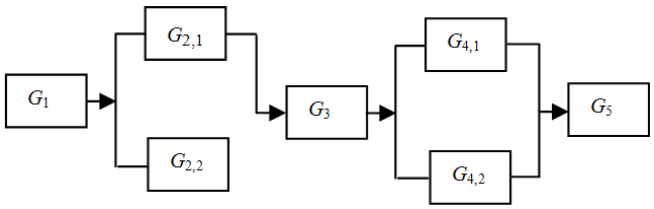

Fig. 6. Group section contours of hip bone according to four outer fork-like positions. In these groups, i in G_i denotes the numerical order of the slice group. If there is only a contour group in a slice group, G_i denotes the contour group. If there are several contour groups in a slice group, k in $G_{i,k}$ denotes the numerical order of the contour group.

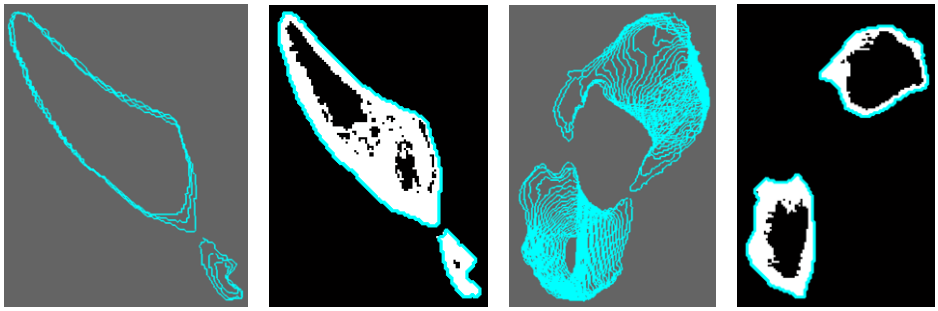

(a) (b) (c) (d)

Fig. 7. Contour groups in same slice groups. (a) $G_{2,1}$ and $G_{2,2}$; (b) two contours in the same a slice while respectively in $G_{2,1}$ and $G_{2,2}$; (c) $G_{4,1}$ and $G_{4,2}$; (d) two contours in the same a slice while respectively in $G_{4,1}$ and $G_{4,2}$.

2.2.2. Inner fork-like position

In the G_3 shown in Figure 6, there is a pair of slices in which the shapes of the contours of the hip bone have a distinct difference: the contour of the acetabulum changes from an inner contour to a part of the outer contour, as shown in Figure 8. The pair of slices is called an inner fork-like position in this paper. The two contours can't use the same anatomical structure because of the shape difference in the inner fork-like position. Consequently, the group should be divided into two groups in the inner fork-like position.

Note that only outer contours are extracted by the method in sub-section 2.1 (see Figure 4). That is, there is no inner contour information that can be used when we divide G_3 into two groups. In order to

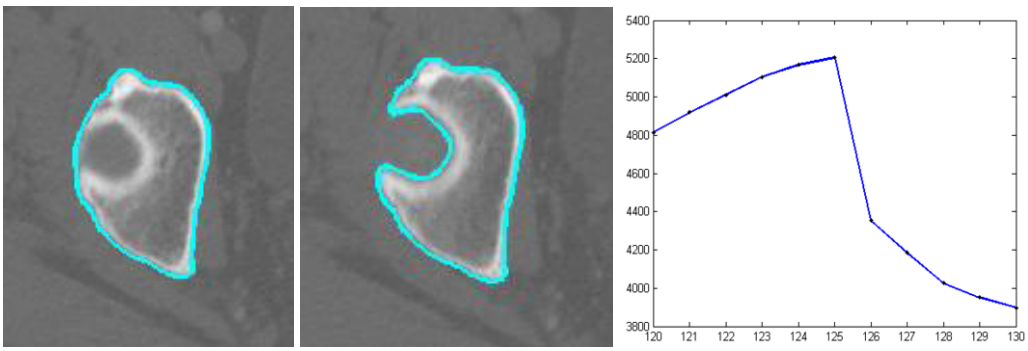

(a) (b) (c)

Fig. 8. Inner fork-like positions of hip bone contours. (a) and (b): top of acetabulum; (c) areas(number of pixels) of regions limited by contours in some successive slices. Horizontal axis: position of slice; vertical axis: area

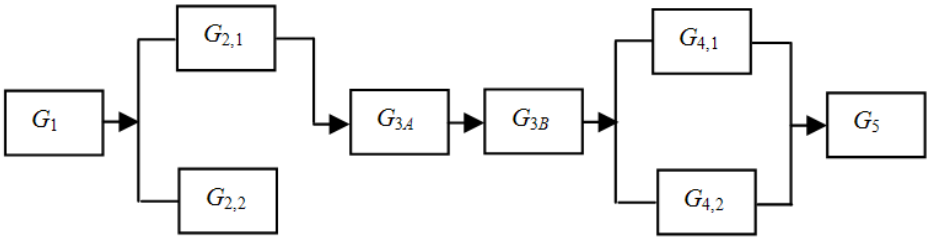

Fig.9. Group section contours of hip bone. In these groups, i in G_i denotes the numerical order of the slice group. If there is a contour group in a slice group, G_i denotes the contour group. If there are several contour groups in a slice group, k in $G_{i,k}$ denotes the numerical order of the contour group. A and B are obtained according to the inner fork-like position.

automatically recognize the inner fork-like position, the area of every region limited by these contours is computed. The relation curve between areas and slice serial numbers is obtained as shown in Figure 8(c). If there is a maximum area leap between an adjacent slice pair (S_{k-1}, S_k), the slice pair is an inner fork-like position. Figure 9 gives a new group relation.

2.3. DCSS construction

2.3.1. Curve gauss smooth

Assuming that $\boldsymbol{C}\{\boldsymbol{p}_0,\ldots,\boldsymbol{p}_n\}$ is a contour, where $\boldsymbol{p}_{n+i}=\boldsymbol{p}_i$ (i=0,1,….,n), it can be smoothed using the following equation:

$$p_i^t=\sum_{w=-k}^{w=k} p_{i+w}^{t-1} g(w,\sigma), i=0,1,\cdots,n,$$

where $p_j^0=\boldsymbol{p}_i$, $\boldsymbol{C}^t$ is defined by $\{p_0^t,\ldots,p_n^t\}$. $g(w,\sigma)$ is defined as in Table 1 that is a discrete format of the Gaussian kernel:

$$g(w,\sigma)=exp(-w^2/2\sigma^2)/(\sigma\sqrt{2\pi})$$

Table 1

Gauss smooth window (σ=1.0)

w	-4.0	-3.0	-2.0	-1.0	0.0	1.0	2.0	3.0	4.0
$g(w,\sigma)$	0.001	0.0044	0.0540	0.2420	0.3989	0.242	0.0540	0.0044	0.001

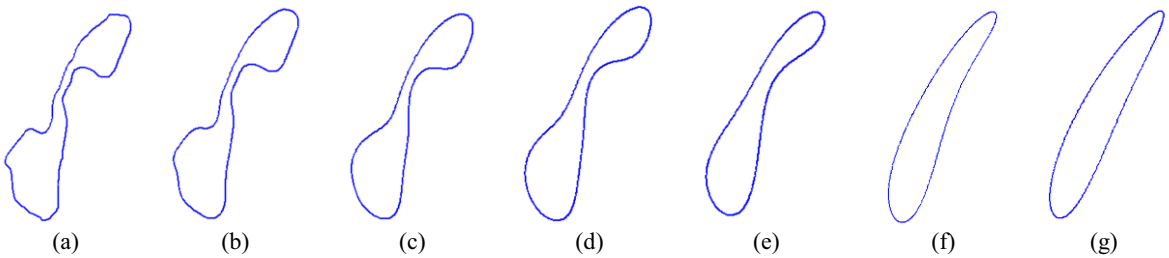

(a) (b) (c) (d) (e) (f) (g)

Fig. 10. Curves under different smooth steps. (a) t= 3; (b) t= 20; (c) t= 100; (d) t= 500; (e) t= 800; (f) t= 2500; (g) t= 4000.

The weights in Table 1 are obtained under scale σ=1.0. Other weight tables can be also obtained using other scales. For a fixed smooth window, the larger the parameter t is, the smoother the contour C^t is. Figure 10 gives an example of how the contour $\boldsymbol{C}^t$ evolves when the parameter t increases.

2.3.2. DCSS

DCSS was presented by Zhong, et al. [23] and used to recognize corners (curvature extreme point) in contours. See Figure 11, a DCSS consists of curves, one of which is a track curve of a corner under a different contour C^t (t = 0,1,…). That is, a point (s,t) in a DCSS curve means that the s-th point is a corner for the contour C^t. To extract corners using DCSS two parameters must be chosen: (1) smooth step number t, that is, under what curve smooth degree corners should be extracted; (2) magnitude of curvature absolute value, that is, how large the curvature of a point should be when it is regarded as a corner. Since our method takes in account anatomical properties of contours as prior knowledge, extracted corners in this work don't depend on such parameter choices.

2.3.3. Anatomical structure reveal in DCSS

A coordinate image system is used to distinguish the inner side and the outer side of hip bones, as shown in Figure 12. According to the orientation of the pelvis in the CT images, the left/right side is also defined.

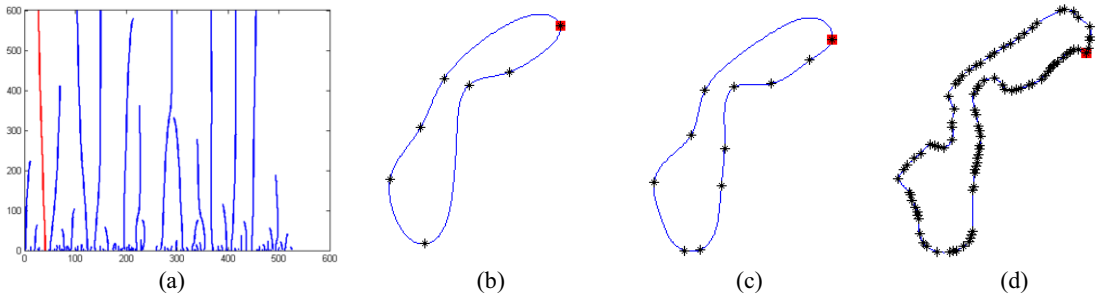

Fig. 11. Direct curvature scale space (DCSS). (a) DCSS curves. Red curve: investigated curve. Horizontal axis: arc parameters of points in the contour. Vertical axis: smooth steps. (b) contour and corners under t = 600; (c) contour and corners under t = 300; (d) contour and corners under t = 1. black star: corner; red square: corners correspond to the red curve in (a).

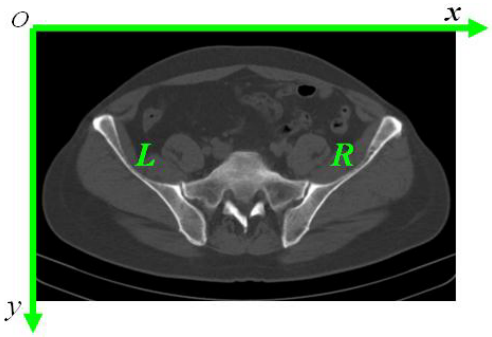

Fig. 12. Coordinate system of CT and definitions of left and right. For the left hip bone, every point in its inner side contour has the normal vector whose dot product with the positive direction of the x axis is superior to zero; For the right hip bone, every point in its inner side contour has the normal vector whose dot product with the positive direction of the x axis is inferior to zero.

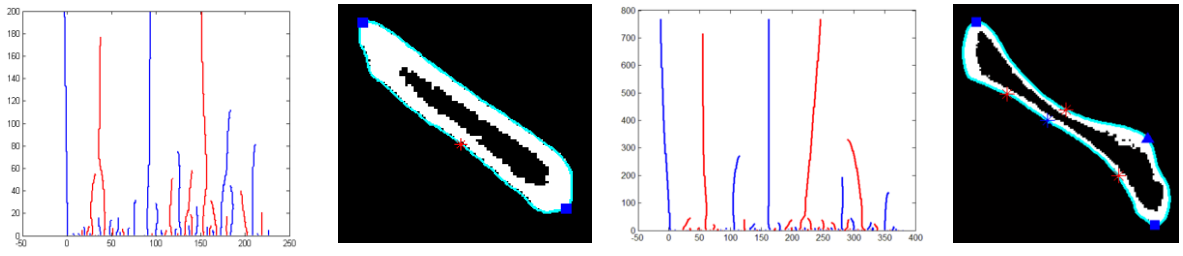

(a) (b) (c) (d)

Fig. 13. DCSS and corners in G_1. (a) DCSS shows that there are two useful corners; (b) corners obtained under a smooth step. (c) DCSS show that there are three useful corners; (d) corners obtained under a smooth step. Blue square: two principal corners; Blue triangle: corner newly identified; star: unnecessary corners.

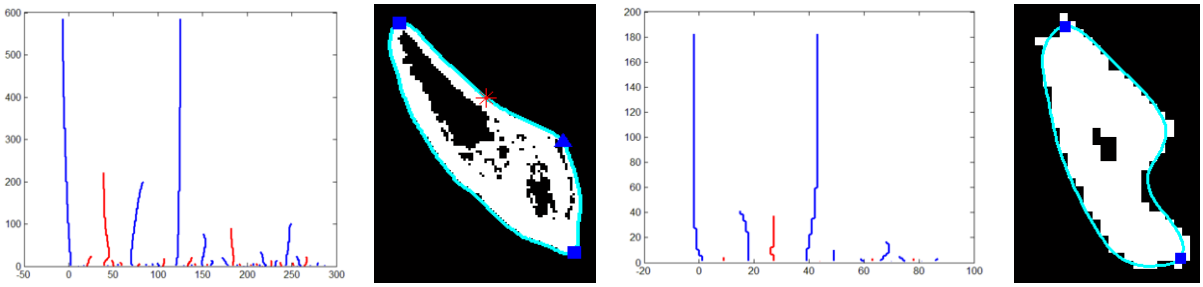

(a) (b) (c) (d)

Fig. 14. DCSS and corners in G_2. (a) DCSS shows that there are three useful corners; (b) corners obtained under a smooth step; (c) DCSS shows that there are two useful corners; (d) corners obtained under a smooth step. Blue square: two principal corners; star: unnecessary corners.

● Group 1(G_1): There are two distinct convex corners and a large concave region (see Figures 1 and 13). The two convex corners are fringe points of the anterior side and the posterior side of the hip bone, see blue square in Figures 13(b) and 13(d). The large concave region is the fossa iliaca (see Figures 1 and 13(d)). Except for the two distinct convex corners, there is also a demarcation line between the fossa iliaca and the auricular surface. It is in the inner side of the hip bone.

Investigate contours from top to bottom. The intersection point between the demarcation line and the slice plane gradually appears. It is a convex point on the hip surface. Sequentially, the convex point evolves into two convex points: one for the arcuate line and one for the boundary of the auricular surface. Therefore, anatomical properties of Group 1 in the DCSS are two convex points in the two ends of the hip bone, which are respectively the two most convex points. There is another 1~2 distinct convex and a concave point on the inner side of hip bone, see Figure 13. From top to bottom, the number of convex points in the hip's inner side gradually increases.

● Group 2.1($G_{2,1}$) and Group 2.2($G_{2,2}$): The shapes and relative positions of the contours in the two groups are shown in Figure 7. Anatomical properties of Group 2.1 in the DCSS are the greater sciatic notch and the arcuate line; and the hip fringe around the anterior inferior iliac spine. The first two are the two principal corners. Anatomical properties of Group 2.2 in the DCSS are the hip fringe around the posterior inferior iliac spine and the greater sciatic notch. The two points are the two principal corners, as shown in Figure 14.

● Group 3A($G_{3,A}$) and Group 3B($G_{3,B}$): There are 2~3 convex points in Group 3A: the hip fringe around the anterior inferior iliac spine (probably), the arcuate line/ pecten pubis and the greater sciatic notch, as shown in Figures 15(b) and 15(d). The difficulty of only using DCSS to recognize the 3

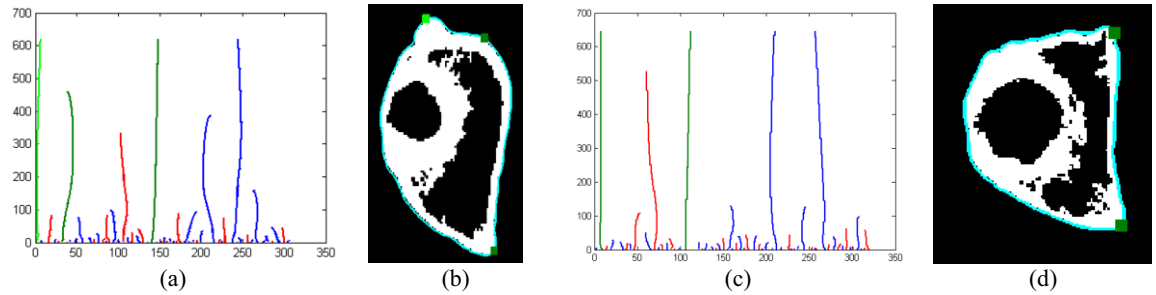

(a) (b) (c) (d)

Fig. 15. DCSS and corners in G_{3A}. (a) DCSS shows that there are three useful corners; (b) corners obtained under a smooth step; (c) DCSS shows that there are two useful corners; (d) corners obtained under a smooth step. Green: useful corners; dark green: the arcuate line/ pecten pubis, the greater sciatic notch; light green: hip fringe around the anterior inferior iliac spine.

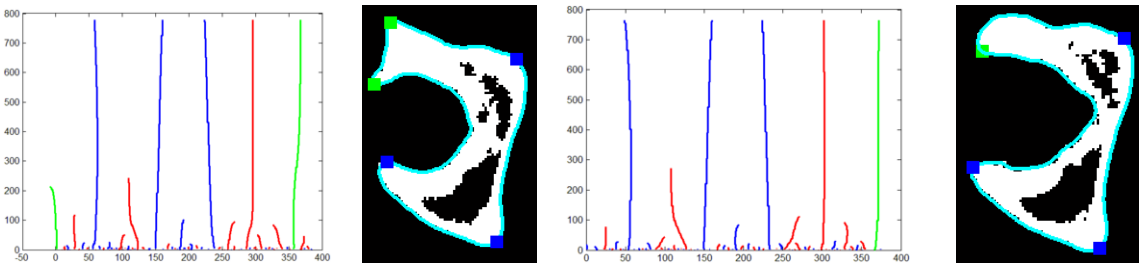

(a) (b) (c) (d)

Fig. 16. DCSS and corners in G_{3B}. (a) DCSS shows that there are 4 useful corners (green and blue); (b) corners obtained under a smooth step; (c) DCSS shows that there are 4 useful corners; (d) corners obtained under a smooth step. Green: a acetabulum fringe around which a hip fringe probably exists.

anatomical feature points is that the first point doesn't necessarily exist. This problem can be solved by the fact that the two main feature points are on the fringe of the hip bone, while another feature point is on the inner side of the hip bone. From Figure 15(b), it can be also said that the intensity of the hip fringe around the anterior inferior iliac spine is weak. Indeed, it will become weaker until it disappears in the subsequent slices (see Figure 16).

In Group 3B, there are generally 4 main convex points (see Figure 16): the pecten pubis, hip fringe around the greater/lesser sciatic notch, and two points in the acetabulum fringe However, there are other feature points, as the hip fringe around the anterior inferior iliac spine (see Figure 16). In order to simplify our discussion, we neglect such minor feature points even though it is not a difficult task to find these feature points according to the END type corner principle [23] (see Figures 16(a) and 16(b)).

● Group 4.1 ($G_{4,1}$) and Group 4.2 ($G_{4,2}$): Shapes and relative positions of the contour in the 2 groups are shown in Figure 17. There are 2~3 main convex points in the Group 4.1: one for the obturator foramen and the other 1~2 for the boundaries of the pubic symphysis surface. In the Group 4.2, there are 2~3 lasting feature points. One is the obturator foramen and another is the lesser sciatic notch (or a boundary of the ischial tuberosity surface). If there is another convex last point, it is a fringe point of the acetabulum, or another boundary of the ischial tuberosity surface. When the fringe point of the acetabulum disappears, another feature point—a boundary of the ischial tuberosity surface-becomes stronger. It is not difficult to distinguish such feature points according to their positions in the contours.

● Group 5(G_5): the corner distribution is the simplest in the group with only 2 main corners in the contours. They are feature points of the ischial ramus.

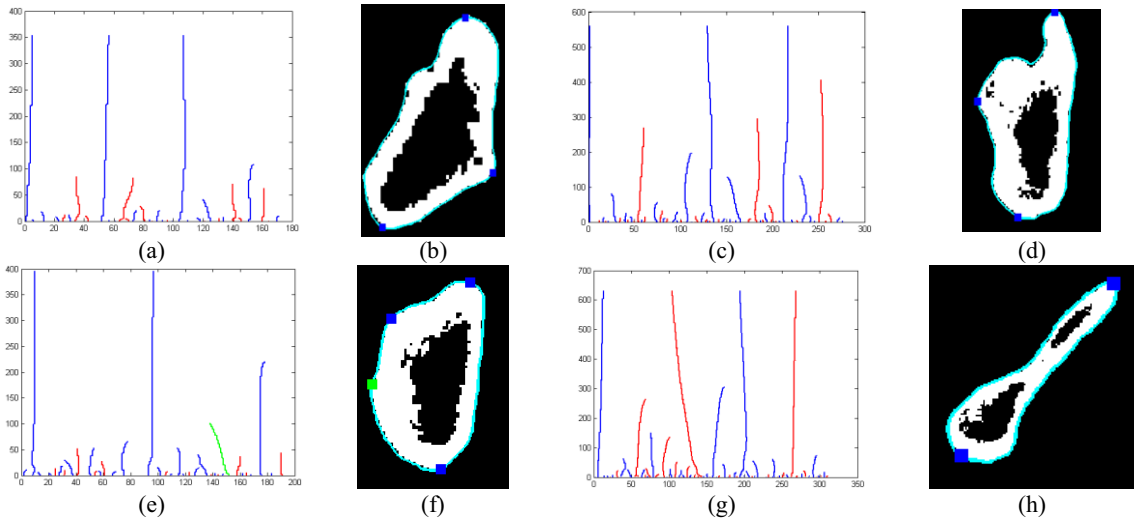

Fig. 17. DCSS and corners in G_4 and G_5. (a) and (b): DCSS and recognized corners of a contour in $G_{4,1}$; (c) and (d): DCSS and recognized corners of a contour in $G_{4,2}$; (e) and (f): DCSS and recognized corners of another contour in $G_{4,2}$; (c)~(f) show that a fringe point of the acetabulum disappears while a boundary of the ischial tuberosity surface becomes stronger from top to bottom for $G_{4,2}$. (g) and (h): DCSS and recognized corners of a contour in G_5. There are only 2 main corners.

Table 2

Anatomical feature point number in every contour

	G_1	G_2		G_3		G_4		G_5
		$G_{2,1}$	$G_{2,2}$	G_{3A}	G_{3B}	$G_{4,1}$	$G_{4,2}$	
number	2~3	3	2	3~2	5~4	3~2	3~4	2
position	inner	global	end	inner	global	inner	outer	end
property	convex	convex	convex	convex	convex	convex	convex	convex

Note: n_1~n_2 means that there are n_1 to n_2 corners in each contour from top to bottom. Inner means there are corners on the inner side and two ends. Outer means that there are corners on the outer side and two ends. Global means that corners are distributed on the whole contour. Convex means that corners are convex.

From the above analysis, it can be said that the role of the corner number is equivalent to the role of the curvature thresholds in [23]. In this paper, the anatomical structure is used to show the corner number in every contour. Table 2 shows the corner number in every contour.

2.3.4. Corner link

In sub-section 2.3.3, all anatomical feature points have been obtained and labeled in every contour: fringe points of the hip bone, points in the demarcation line between the fossa iliaca and the auricular surface, fringe points of the acetabulum, arcuate line/pecten pubis, obturator foramen and boundaries of the pubic symphysis surface. These feature points with same labels in every two adjacent slices are linked. After that, anatomical feature curves appear.

Due to data noise and sampling errors, these feature curves aren't smooth, which means they are zig-zag curves. This is a common drawback in feature curve extractions [28, 29]. We use the method in [29] to smooth these zig-zag curves. Figure 18 shows comparisons between zig-zag curves and smooth curves.

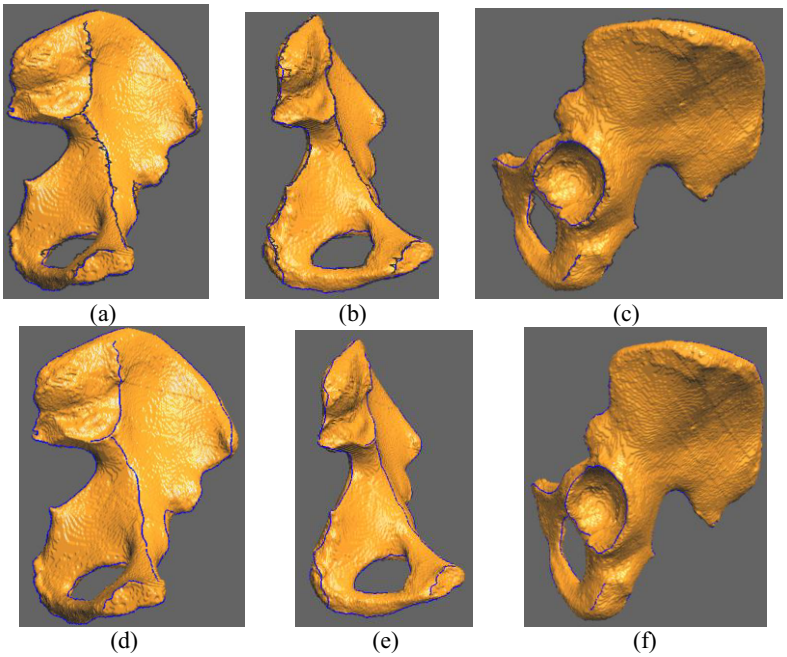

Fig. 18. Comparisons between zig-zag curves and smooth curves. (a)~(c): zig-zag curves (black) and smooth curves (blue); (d)~(f): smooth curves.

3. Experiments and analysis

Our algorithm is implemented using Matlab (version 2007) in a PC with two 1.8 G CPU and 2.0 G RAM. The extracted feature curves are rendered in a software tool developed using VC++2008.

3.1. Smooth step number

The smooth step number is the key factor for the time-consuming character of the algorithm. Since every normal hip bone has a similar shape, a normal adult hip bone is used to determine the smooth step number. CT image parameters of the hip bone are listed in Table 3. The smooth step numbers for each group are listed in Table 4. The table shows that the feature recognizing technique in this paper only needs small smooth step numbers, which means our algorithm is less time-consuming. It should be noted that a similar CSS technique needs a certain smooth step number so that concave regions disappear [22]. Unlike the technique that uses DCSS to extract corners, which needs given smooth step numbers and curvature thresholds, our method doesn't depend on any manual parameter choices.

3.2. Accuracy evaluation

Table 3

CT parameters of the used hip bone

Slice Number	Image Size(pixel)	Slice Spacing(mm)	Pixel Spacing(mm)
215	512×512	0.6777	1.0

Table 4

Smooth step number statistics

	G_1	G_2		G_3		G_4		G_5
		$G_{2,1}$	$G_{2,2}$	G_{3A}	G_{3B}	$G_{4,1}$	$G_{4,2}$	
Contour	94	3	3	28	43	27	27	20
Max.	413	527	61	635	516	213	248	356
Min	173	213	48	229	249	117	132	106
Average	296	394	53	471	391	152	164	193
Time(s)	5.3214	0.6177	0.0732	2.4651	3.9621	1.4361	1.5893	1.2175

Note: Contour means Average Contour Number; Max, Min and Average respectively mean Max, Min and Average smooth steps. Time means Time Consuming.

In order to evaluate the accuracy of extracted feature curves (denoted by set A), we invited three surgeons to interactively construct AFC. The average position is used as a reference standard (denoted by set B). Firstly, we re-sampled the reference curve and extracted feature curves with a pixel spacing in Table 3. In all later discussions, re-sampled curves were used. In order to make convenient and accurate comparisons, a basic concept is used: the counterpart point. Let $S(A)$ denote the points of A. Let $S(B)$ denote the points of B. For a point s_A in the set $S(A)$, compute its closest point s_B in the set $S(B)$ in the Euclidean distance. Assume that the feature curve that passes through s_A is c_A and that the one which passes through s_B is c_B. If c_A and c_B have the same anatomical label (see subsection 2.3.4) and the distance

$$| s_A\, s_B| \le d_T,$$

where d_T is a given parameter, set as 5.0 mm, that is about a measure error upper limit [1], s_A and s_B are counterpart points of each other. Feature curves extracted by our algorithm are compared with the reference standard in the following aspects:

- Dice coefficient: The Dice coefficient between two sets of pixel A and B is defined as:

$$DC(S(A),S(B)) = 2(S(A)\cap S(B))/(S(A)+S(B))$$

where if $s_A \in (S(A)\cap S(B))$, s_A has a counterpart point s_B and s_B has also its counterpart point s_A. The Dice coefficient is 1 for a perfect AFC set and 0 if extracted curves and the reference do not overlap at all.

- Average symmetric surface distance (*ASD*): The shortest distance of a point v to $S(A)$ is defined as:

$$d(v, S(A)) = \min_{s_A \in S(A)} | v - S(A) |$$

The metric represents these distances' average measure, which is 0 for a perfect extraction:

$$ASD(A,B) = \frac{1}{| S(A) | + | S(B) |} \left(\sum_{s_A \in S(A)} d(s_A, S(B)) + \sum_{s_B \in S(B)} d(s_B, S(A)) \right)$$

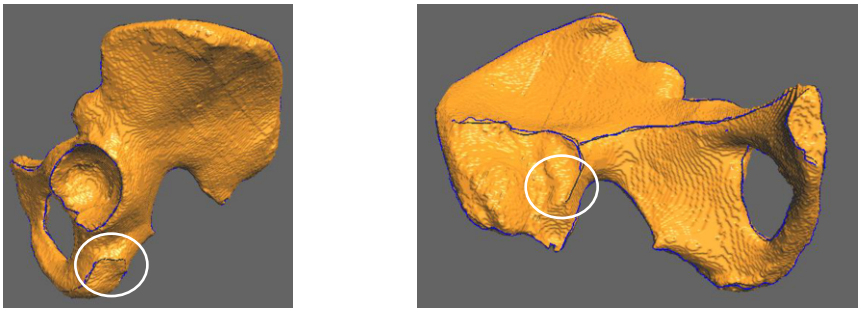

(a) (b)

Fig. 19. Comparison between feature curves delineated by a surgeon and feature curves extracted in this paper. (a) inner side; (b) outer side. Black: curves delineated by surgeons; blue: curves extracted by our method. Parts in white circles: feature curves missed by our method.

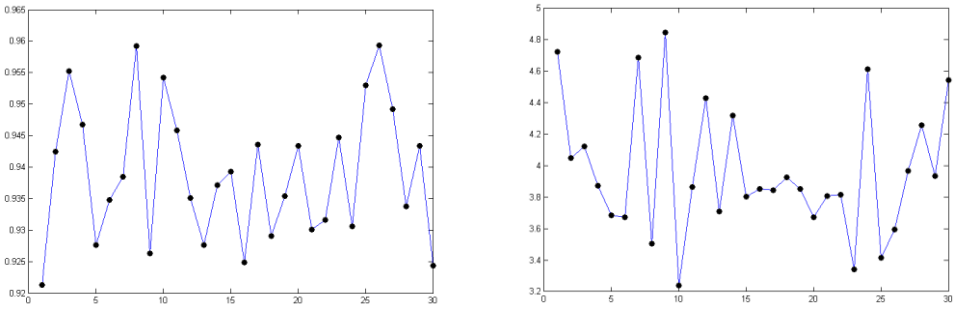

(a) (b)

Fig. 20. Accuracy evaluation for our method using 30 hip bones. (a) Dice coefficient; (b) average symmetric surface distance.

We collected 30 hip bones (see sub-section 2.1) to evaluate the accuracy of our algorithm. Figure 19 gives a comparison between feature curves delineated by surgeons and feature curves extracted in this paper. From Figure 19, it can be seen that several feature curve parts are missed by our method. Those feature curve parts are approximately parallel to slice planes, which is a disadvantage of our method. However, there are very little curve parts. Locating anatomical landmarks isn't affected by these missed curve segments. Figure 20 gives two curve diagrams of the Dice coefficient and ASD for every case. The two diagrams show that the Dice coefficient and the ASD, respectively, range 0.92~0.96 and 3.24 mm~4.85 mm. The last one is less than the common range [1]. The two diagrams show that our method is robust for various normal adult hip bones.

3.3. Comparison with similar works

The curvature-based method is a typical method to extract feature curves of surfaces [1] in 5 procedures:

Table5

Patch classification using curvatures

(H>0,K>0)	(H>0,K=0)	(H>0,K<0)	(H<0,K>0)	(H<0,K=0)	(H<0,K<0)
1	2	3	4	5	6

Step 1: get clusters $C_i \subset \Omega_v$, $\{i = h, l\}$ according to their H value (mean curvature) by given thresholds CT_{max} and CT_{min}. Ω_v is the vertex set of the model surface represented by a triangle mesh.

Step 2: form groups $G_i \in C_h$, $\{i = 1, 2, 3\}$ and $G_i \in C_l$, $\{i = 4, 5, 6\}$ from corresponding clusters using K, as shown in Table 5.

Step 3: construct triangle seed lists $S_{ij} \in G_i$, $\{i = 1,2, \ldots, 6; j = 1,2, \ldots, M\}$.

Step 4: get landmark regions $R_{ijk} \in S_{ij}$, $\{i=1,2, ...,6; j=1,2, ..., M; k=1,2, ..., N\}$ by segmenting homogenous triangles in particular seed lists according to the following equation:

$$LR_i = 1 + 3(1 + sgn(H, \varepsilon)) + (1 - sgn(K, \varepsilon))$$

where,

$$sgn(x,\varepsilon) = \begin{cases} +1, & x > \varepsilon \\ 0, & |x| \le \varepsilon \\ -1, & x < \varepsilon \end{cases}$$

Step 5: filter regions out by surface area, geometric characteristics of the associated triangles and spatial location of the region, taking into consideration the required landmarks according to the spatial adjacency matrix of those landmarks.

In step 1, two given thresholds CT_{max} and CT_{min} are needed. In fact, as far as the hip bone is concerned, because the convex/concave region is a relative concept in the sense of palpation and vision, the threshold adjustment probably has some disadvantages: either some regions are missed or there are too many regions. Figure 21 gives a mean curvature distribution histogram for the model described in subsection 3.1. We choose CT_{max} and CT_{min} according to the histogram. In Figures 22(a)-22(e), there are some regions of anatomical landmarks missed; In (c)~(i), there are some regions with uncorrected connectivity. In Figures 22(g)-22(i), there are also too many S_{ij}. When there are too many S_{ij}, too many R_{ijk} appear, which makes area filters and spatial locations difficult.

From Figures 22(d)-22(i), it can be noted that some anatomical landmarks on the fringe of the hip bone have been linked. In this case, the spatial adjacency matrix of landmarks can be used because those landmarks should be separated before using the spatial adjacency matrix. The curvature-based method can work in reference [1] due to the following facts: (1) little slice spacing (0.67 mm) that usually can't be achieved in usual clinical CT scanning (see section 2.1). Little slice spacing results in little noises of the model surface; (2) careful parameter choices: curvature thresholds, surface areas,

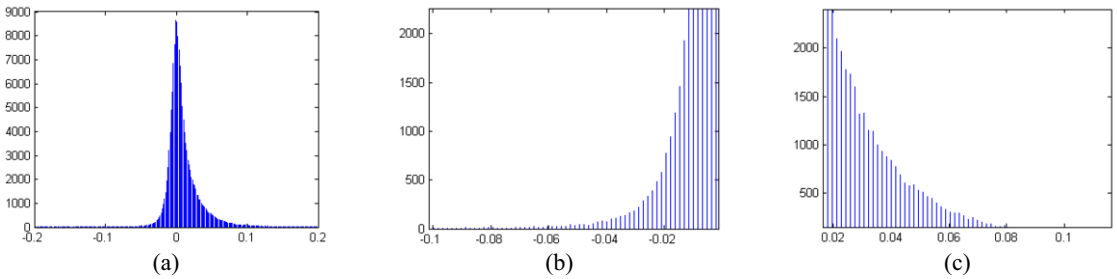

(a) (b) (c)

Fig. 21. Mean curvature distribution histogram for a hip bone surface. (a) whole histogram; (b) local magnification of left side; (c) local magnification of right side.

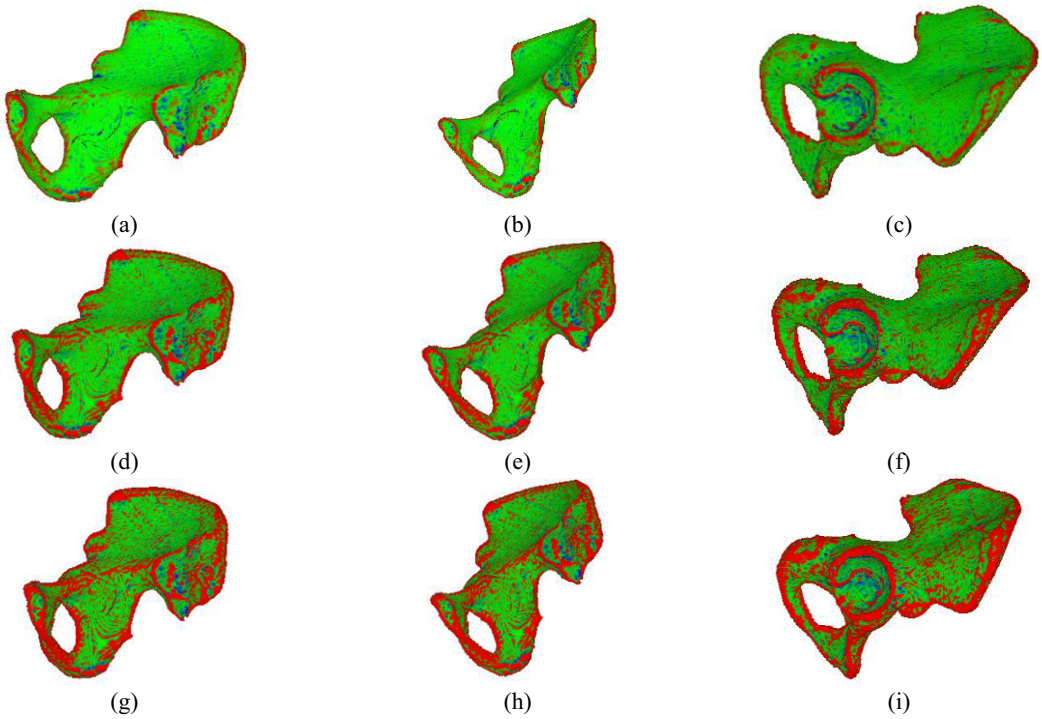

Fig. 22. Segment convex/concave regions using curvature thresholds. (a) ~ (c): CT_{max} = 0.05, CT_{min} = -0.05; (d) ~ (f): CT_{max} = 0.02, CT_{min} = -0.05; (g) ~ (i): CT_{max} = 0.01, CT_{min} = -0.05. red: regions with curvature CT_{max}; blue: regions with curvature CT_{min}; green : regions with curvature 0.

geometric characteristics of the associated triangles, etc. Usually, only experienced users can obtain satisfactory results by adjusting these parameters. (3) Compared with hip bones, there are less anatomical landmarks in the surface of knee bones and those anatomical landmarks can be segmented using a curvature-based method.

3.4. Application

Since anatomical landmarks are conventional landmarks (see Figure 1) in medical science, this section uses AFC extracted in this paper to locate anatomical landmarks. See Figure 1 and Figure 18, there are only 7 anatomical feature curves: one through the iliac crest, the posterior superior iliac spine, the posterior inferior iliac spine, the greater sciatic notch, the ischial spine, the lesser sciatic notch, the ischial tuberosity, the ischial ramus, the tuberculum pubicum, the anterior inferior spine and the anterior superior spine; the demarcation line between the fossa iliaca and the auricular surface; the fringe of the acetabulum; the obturator foramen, the arcuate line, a boundary of the pubic tubercle and a boundary of the ischial tuberosity.

The last 6 curves are anatomical landmarks themselves. So the task is to locate anatomical landmarks using the first feature curve. For convenience, we name the curve as the fringe of the hip bone and denote it as Γ. Because a 3D curve is more complex than a 2D curve, the fringe of the hip bone is projected to the *yoz* plane (sagittal plane, see Figure 3(b)). According to the anatomical structure (see Figure 1), there are 11 main corners: the iliac crest, the posterior superior iliac spine, the posterior inferior iliac spine, the greater sciatic notch, the ischial spine, the ramus ossis ischiin, the

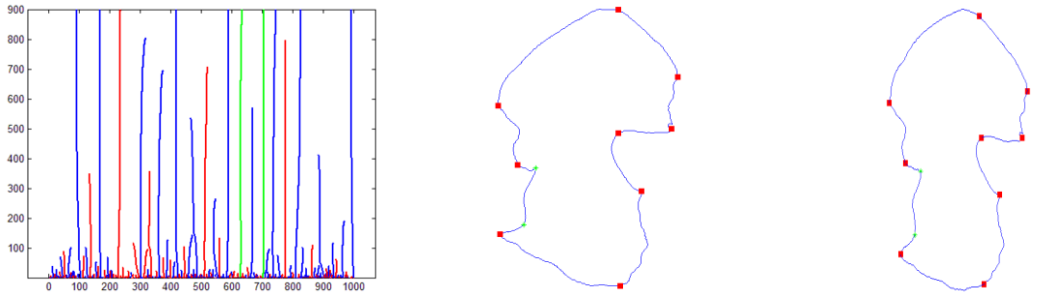

(a) (b) (c)

Fig. 23. Location of anatomical landmarks on the fringe of hip bone. (a) DCSS of the projection on *yoz* plane. (b) projection on *yoz* plane of the fringe of hip bone; (c) real fringe of hip bone that is a 3D curve. Green: LM1, LM2 and their DCSS curves; red square: recognized landmarks

pubic tubercle, LM1, LM2, the anterior inferior spine and the anterior superior spine. We smooth the projection contour in the *yoz* plane till there are 11 corners (see Figure 23). Therefore, these anatomical landmarks can be located.

4. Conclusions

Based on the DCSS corner recognizing technique in computer graphics, this paper presents a method to automatically extract AFC from hip bone surfaces that are represented by section contours parallel to the horizontal plane. In this method, the anatomical structure is used as prior knowledge when grouping section contours and when recognizing feature points in section contours.

Compared with traditional feature curve extraction methods, advantages of our method include: (i) no parameter choices; (ii) no redundant feature curves; (iii) excellent anti-noise performance. These advantages derive from two basic principles: (i) use of a multi-scale technique to recognize corners; (ii) foreknowledge of the main corners in each contour based on the anatomical structure. Applications show that the anatomical feature curves extracted by our method can be used to automatically and accurately locate conventional anatomical landmarks.

Consequently, this paper gives a novel method to accurately extract anatomical feature curves and to locate anatomical landmarks without any parameter choices for normal hip bones. In further work, we will apply this method to other organs.

Acknowledgment

This work was supported by the National Nature Science Foundation of China under Grant No. 51175248/E050603. Professor Baojiang Zhong from Soochow University and Professor Jun Wang from NUAA were of great help for our work. The manuscript was completed when the first author was a visiting scholar in CISE, of the University of Florida. The supervisor Professor Jörg Peters significantly encouraged and assisted our work.

References

[1] K. Subburaj, B. Ravia and M. Agarwal, Automated identification of anatomical landmarks on 3D bone models reconstructed from CT scan images, Computerized Medical Imaging and Graphics **33** (2009), 359–368.
[2] J. Ehrhardt, H. Handels, T. Malina, et al., Atlas-based segmentation of bone structures to support the virtual planning of hip operations, International Journal of Medical Informatics **64** (2001), 439–447.
[3] X. Zhang, Y. Zhu, C. Li, et al., SIFT algorithm-based 3D pose estimation of femur, Bio-Medical Materials and Engineering **24** (2014), 2847–2855.
[4] H. Handels, J. Ehrhardt, W. Plotz, et al., Virtual planning of hip operations and individual adaption of endoprostheses in orthopaedic surgery, International Journal of Medical Informatics **58** (2000), 21–28.
[5] F. Li and Z. Song, Surface-based automatic coarse registration of head scans, Bio-Medical Materials and Engineering **24** (2014), 3207–3214.
[6] K.T. Rajamania, M.A. Gonzalez, L.P. Nolte, et al., A novel and stable approach to anatomical structure morphing for enhanced intraoperative 3D visualization, Proceedings of SPIE-the International Society for Optical Engineering, Los Angeles, USA, 2005, pp. 637–646.
[7] P. Foroughi, D. Song and G. Chintalapani, Localization of pelvic anatomical coordinate system using atlas registration for total hip replacement, Medical Image Computing and Computer-Assisted Intervention **11** (2008), 871–879.
[8] C.G. Zhang, T.C. Huang and T. Guerrero, Use of three-dimensional (3D) optical flow method in mapping 3D anatomic structure and tumor contours across four-dimensional computed tomography data, Journal Application Clinical Medical Physics **9** (2008), 2738–2749.
[9] W. Sun, B. Starly and J. Nam, Bio-CAD modeling and its applications in computer-aided tissue engineering, Computer-Aided Design **37** (2005), 1097–1114.
[10] A. Werner, Z. Lechniakb and K. Skalski, Design and manufacture of anatomical hip joint endoprostheses using CAD/CAM systems, Journal of Materials Processing Technology **107** (2000), 181–186.
[11] Y. Jun and K. Choi, Design of patient-specific hip implants based on the 3D geometry of the human femur, Advances in Engineering Software **41** (2010), 537–547.
[12] V. Sint and S. Jan, Color atlas of skeletal landmark definitions: Guidelines for reproducible manual and virtual palpations, Churchill Livingstone Press, Elsevier, 2007.
[13] Q. Zhou, T. Weinkauf and O. Sorkine, Feature-based mesh editing, Proceeding Eurographics, 2011, pp. 214–218.
[14] T. Varady, A. Michael and T. Zsolt, Automatic extraction of surface structures in digital shape reconstruction, Computer Aided Design **39** (2007), 379–388.
[15] M.A. Styner, K.T. Rajamani and L. Nolte, Evalation of 3D correspondence methods for model building, Information Processing in Medical Imaging **32** (2003), 63–75.
[16] H. Seim, D. Kainmueller and M. Heller, Automatic segmentation of the pelvic bones from CT data based on a statistical shape model, in: Eurographics Workshop on Visual Computing for Biomedicine, C.P. Botha, ed., Cambridge University Press, London, 2008, pp. 93–100.
[17] F. Yokota, T. Okada and M. Takao, Automated segmentation of the femur and pelvis from 3D CT data of diseased hip using hierarchical statistical shape model of joint structure, Medical Image Computing and Computer-Assisted Intervention **12** (2009), 811–818.
[18] Y. Ohtake, A. Belyaev and H. Seidel, Ridge-valley lines on meshes via implicit surface fitting, ACM Transactions on Graphics **23**(2004), 609–612.
[19] S. Yoshizawa, A. Belyaev and H. Seidel, Fast and robust detection of crest lines on meshes, Proceedings of the 2005 ACM Symposium on Solid and Physical Modeling, Wales, UK, 2005, pp. 227–232.
[20] T.K. Dey and L. Wang, Voronoi-based feature curves extraction for sampled singular surfaces, Computers & Graphics **37** (2013), 659–668.
[21] M. Kolomenkin, I. Shimshoni and M. Kolomenkin, Multi-scale curve detection on surfaces, IEEE Conference on Computer Vision and Pattern Recognition, Seattle, USA, 2013, pp. 225–232.
[22] F. Mokhtarian and M. Bober, Curvature Scale Space Representation: Theory, Applications, and MPEG-7 Standardization, Springer Press, New York, 2003.
[23] B. Zhong and W. Liao, Direct curvature scale space: theory and corner detection, IEEE Transactions on Pattern Analysis & Machine Intelligence **29** (2007), 508–512.
[24] V. Vidal and C. Wolf, Robust feature line extraction on CAD triangular meshes, International Conference on Computer Graphics Theory and Applications, Vilamoura, Portugal, 2011, pp. 106–112.
[25] K. Demarsina, D. Vanderstraetenb, T. Volodinea, et al., Detection of closed sharp edges in point clouds using normal estimation and graph theory, Computer Aided Design **39** (2007), 276–283.
[26] A. Hubeli and M. Gross, Multi-resolution feature extraction for unstructured meshes, IEEE Proceedings on Visualization, San Diego, USA, 2001, pp. 287–294.
[27] S. Fleishman, D. Cohen and C.T. Silva, Robust moving least-squares fitting with sharp features, ACM Transactions on

Graphics **24** (2005), 544–552.
[28] J. Daniels, L.K. Ha and T. Ochotta, Robust smooth feature extraction from point clouds, IEEE International Conference on Shape Modeling and Applications, Lyon, France, 2007, pp. 123–136.
[29] S. Gumhold, X. Wang and R. Macleod, Feature extraction from point clouds, Proceedings of the 10th International Meshing Roundtable, Newport Beach, USA, 2001, pp. 213–225.
[30] B. Drerup and E. Hierholzer, Automatic localization of anatomical landmarks on the back surface and construction of a body-fixed coordinate system, Journal of Biomechanics 20 (1987), 961–970.
[31] X. Pennnec, N. Ayache and J.P. Thirion, Landmark-based registration using features identified through differential geometry, in: Handbook of Medical Imaging, I.N. Bankman, ed., Academic Press, U.S., 2008, pp. 499–513.
[32] A.F. Frangi, D. Rueckert and J.A. Schnabel, et al., Automatic construction of multiple-object three-dimensional statistical shape models: Application to cardiac modelling, IEEE Transactions on Medical Imaging **21** (2002), 1151–1166.
[33] C. Izard, B. Jedynak and C.E. Stark. Spline-based probabilistic model for anatomical landmark detection, Medical Image Computing and Computer-Assisted Intervention **9** (2006), 849–856.
[34] Y. Cheng, S. Zhou, Y. Wang, et al., Automatic segmentation technique for acetabulum and femoral head in CT images, Pattern Recognition **46** (2013), 2969–2984.
[35] H. Liu, J. Zhao, N. Dai, et al., Improve accuracy for automatic acetabulum segmentation in CT images, Bio-Medical Materials and Engineering **24** (2014), 3159–3177.